International Journal of Fracture **71:** 1–14, 1995.

Statistical character of the failure of multiphase materials due to high pressure water jet impingement

A.W. MOMBER[1] and R. KOVACEVIC[2]
[1] *WOMA Apparatebau GmbH, Germany, Feodor-Lynen Scholar of the Alexander-von-Humboldt Foundation, Bonn, Germany, at the University of Kentucky*
[2] *Center for Robotics and Manufacturing Systems, University of Kentucky, Lexington, KY 40506, USA*

Received 14 October 1994; accepted 13 December 1994.

Abstract. In this study, fracture experiments on multiphase material samples have been carried out using high speed water jets. Based on fracture geometry measurements and on grain analyses it was found that the fracture of this type of materials by water jet impingement is a highly localized process at low pressure ranges. Beyond a critical pressure range of about 30 times the material's tensile strength a change in the material behaviour was observed. This result is in agreement with a theory suggested by Powell and Simpson. To explain the local character of the failure process, a simplified fracture model is introduced which resulted in a relation between a fracture probability parameter and the fracture width in the damaged materials.

1. Introduction

High energy plain water jets have been used to process brittle multiphase materials, such as rocks and concretes, in the mining and quarrying industry and in civil engineering for some years. Typical applications are recently described by Fowell and Martin [1], Vijay [2], Summers [3], and Momber [4]. Regardless of the wide range of application, the mechanism of destruction of brittle multiphase materials due to plain water jets is not well understood.

The general structure of a plain continuous water jet can be assumed as a three region jet. According to [5], [6] and [7], one can discern a core region, a transition region, and a droplet region. In practice, the jet core region is used to cut and remove materials with pressures greater than 100 MPa. In this region static loading due to a stagnation pressure p_s predominates. The stagnation pressure, which is distributed over the loaded surface, can be estimated using the equation

$$p_s = \tfrac{1}{2} \cdot \rho \cdot \nu_0^2, \tag{1}$$

where p_s is the stagnation pressure, ρ is the fluid density and ν_0 is the jet velocity. The stagnation pressure is distributed over the loaded area after a Gaussian curve. This distribution which is shown in Fig. 1 can be described according to [8] as follows

$$p_s(r) = p_s(0) \cdot \mathrm{e}^{-\alpha^2 \cdot r^2}, \tag{2}$$

where $p_s(0)$ is the stagnation pressure on the jet axis, r is the radial distance from the jet axis and α is a constant depending on the jet diameter. For a jet diameter of 1.0 mm, which is a common value for rock and concrete processing, the pressure is distributed over an area of about 0.8 mm^2. This value suggests that integral macroscopic material properties, such as compressive strength and Young's modulus, can not be used for the evaluation of material resistance against water jet attack. The local conditions, and so the local properties, at the

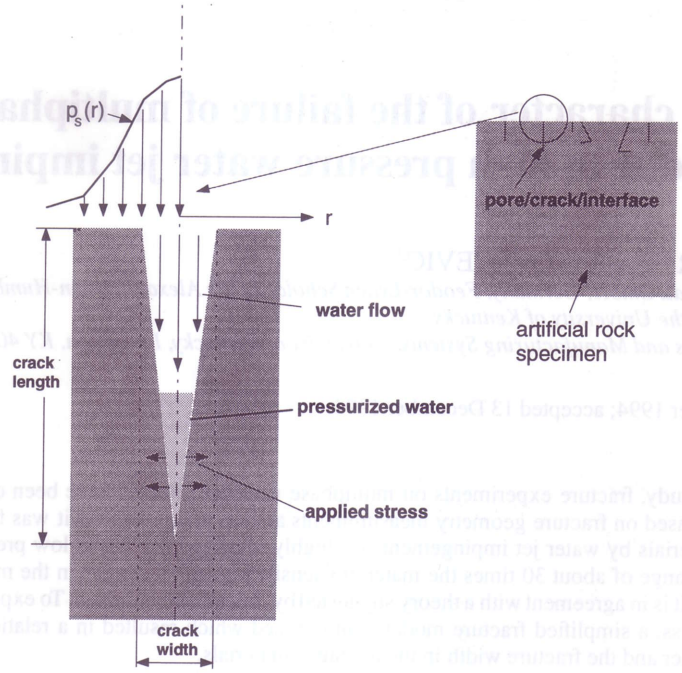

Fig. 1. Mechanism of brittle material destruction by high energy water jet.

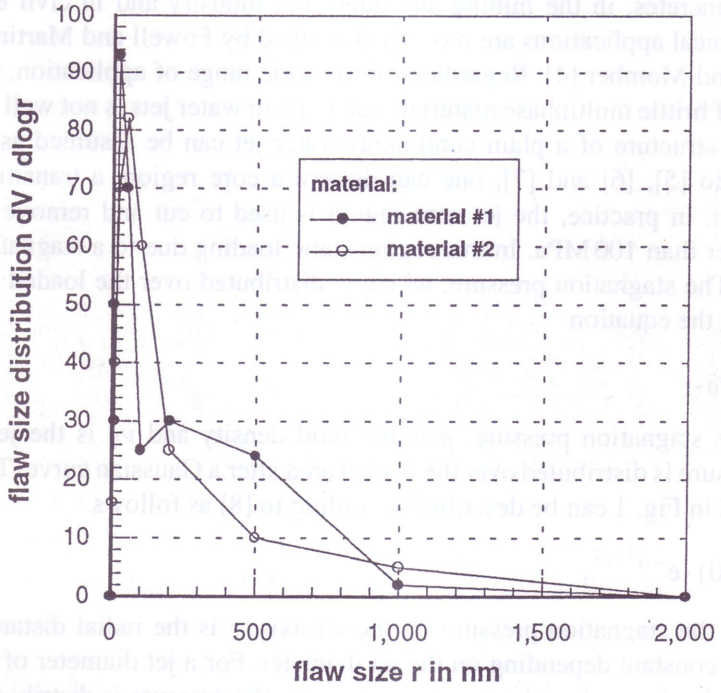

Fig. 2. Results of mercury penetration measurements of two multiphase materials [17].

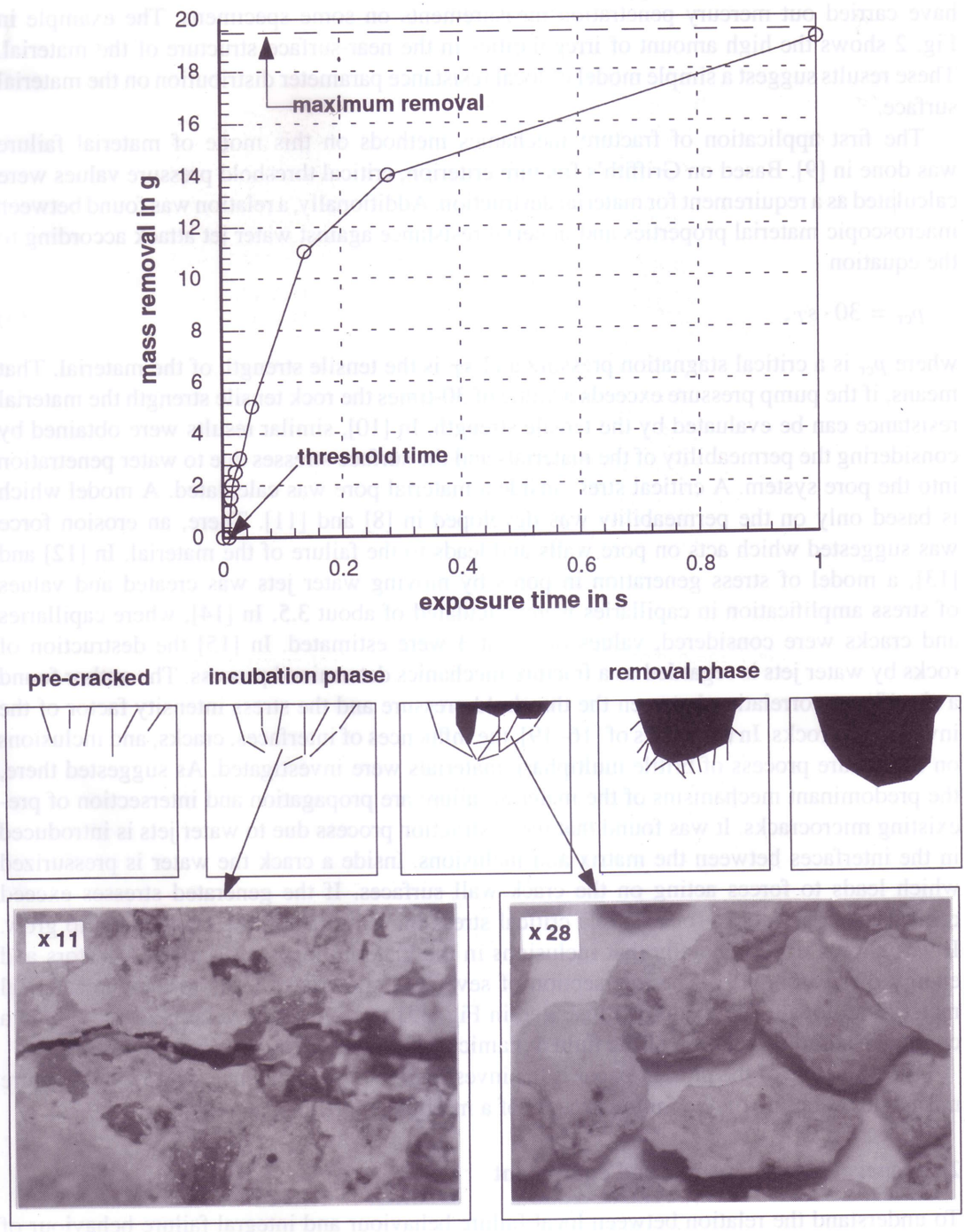

Fig. 3. Generalized water jet removal model for a brittle, multiphase material.

point of impact are of decisive importance for the failure process. This important restriction was not considered consequently in previous investigations of this topic.

Rocks and concretes can be considered as inhomogeneous materials which consist of grains, matrix, interfaces, pores and microcracks. To illustrate this assumption, the authors

have carried out mercury penetration measurements on some specimens. The example in Fig. 2 shows the high amount of irregularities in the near-surface structure of the material. These results suggest a simple model of local resistance parameter distribution on the material surface.

The first application of fracture mechanics methods on this mode of material failure was done in [9]. Based on Griffith's fracture criterion, critical threshold pressure values were calculated as a requirement for material destruction. Additionally, a relation was found between macroscopic material properties and material resistance against water jet attack according to the equation

$$p_{cr} = 30 \cdot s_T, \tag{3}$$

where p_{cr} is a critical stagnation pressure and s_T is the tensile strength of the material. That means, if the pump pressure exceeds a value of 30-times the rock tensile strength the material resistance can be evaluated by the tensile strength. In [10], similar results were obtained by considering the permeability of the materials and the surface stresses due to water penetration into the pore system. A critical stress inside a material pore was calculated. A model which is based only on the permeability was developed in [8] and [11]. There, an erosion force was suggested which acts on pore walls and leads to the failure of the material. In [12] and [13], a model of stress generation in pores by moving water jets was created and values of stress amplification in capillaries were calculated of about 3.5. In [14], where capillaries and cracks were considered, values of about 3 were estimated. In [15] the destruction of rocks by water jets is regarded as a fracture mechanics determined process. The author found a significant correlation between the threshold pressure and the stress intensity factor of the investigated rocks. In the works of [16–19], the influences of interfaces, cracks, and inclusions on the failure process of brittle multiphase materials were investigated. As suggested there, the predominant mechanisms of the material failure are propagation and intersection of pre-existing microcracks. It was found that the destruction process due to water jets is introduced in the interfaces between the matrix and inclusions. Inside a crack the water is pressurized which leads to forces acting on the crack wall surfaces. If the generated stresses exceed critical material values, for example critical stress intensity factor, the crack starts to grow. It was shown experimentally that inclusions in the material may act as crack arrestors and energy dissipators [19]. The intersection of several single cracks leads to a macroscopical material removal. The model is illustrated in Fig. 3. In an advanced version of the model a computer-based calculation of the fluid dynamics inside a microcrack is presented [20].

The objective of the present paper is the investigation of the influence of the *local* fracture mechanics situation on the failure process of a multiphase brittle material.

2. General idea, materials and equipment

To understand the relation between local failure behaviour and integral failure behaviour of multiphase materials, kerfing tests on concrete specimens were carried out with high velocity water jets. After processing, mass removal due to fracture, fracture depth, and fracture width were measured. The general idea behind this investigation is the assumption that especially variations in the width of a generated fracture allow an evaluation of the failure homogeneity. A high standard deviation of this parameter means a high influence of the local material situation and so a high degree of randomness during the fracture process. On the contrary, a low standard deviation could represent a more regular failure over the loaded surface. This

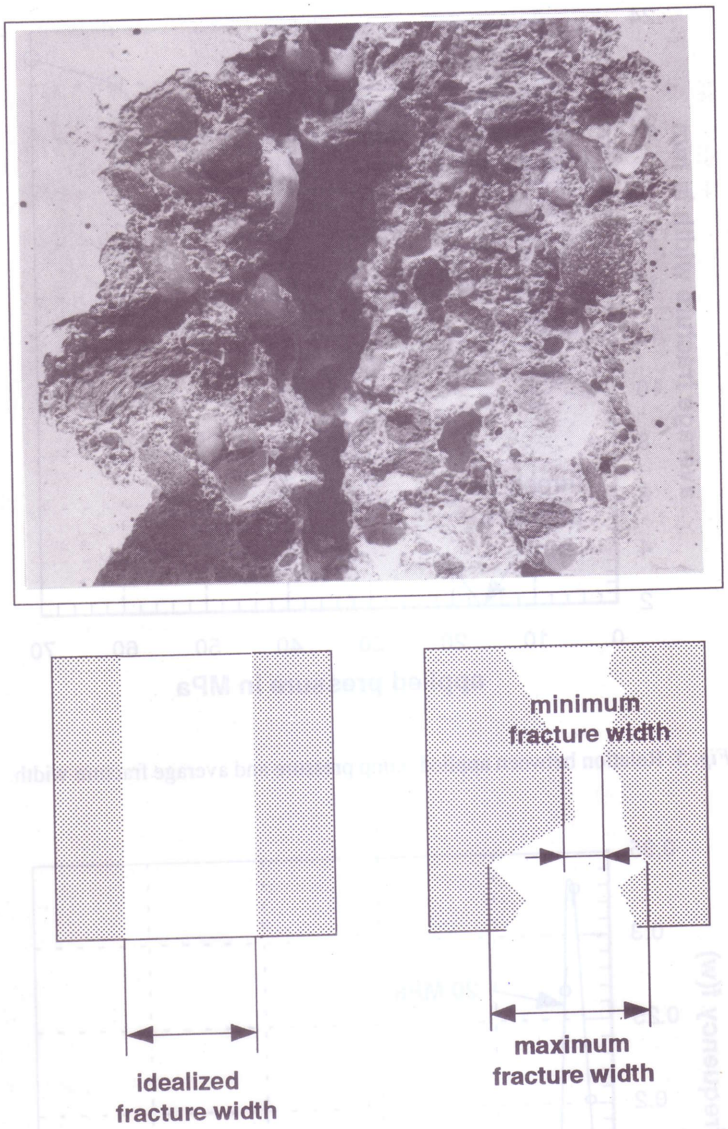

Fig. 4. Ideal and real destruction processes, respectively, in water jet cutting of multiphase brittle materials.

idea is illustrated in Fig. 4. Whereas the fracture width is constant over the fracture length x in an ideal process, this parameter varies in a real cutting performance. The authors suppose that the variations in fracture geometry are not attributed to fluctuations in pump pressure and traverse regime. Two concrete mixtures were designed and tested. They consisted of a hardened mixture of water (w), limestone grains (g) and a binding agent (b). For the latter a portland cement (PZ 35 F) was used. The ratio between water and binder was $w/b = 0.55$. After mixing, these compositions were cured and hardened for 28 days. Table 1 contains selected mechanical properties of the materials.

The high energy water jet unit consisted of a high pressure water pump (110 kW), hose system, nozzle holder, nozzle and rotating worktable. The nozzle holder and specimens were located inside a closed plexiglass cell, so that it was possible to collect the removed material

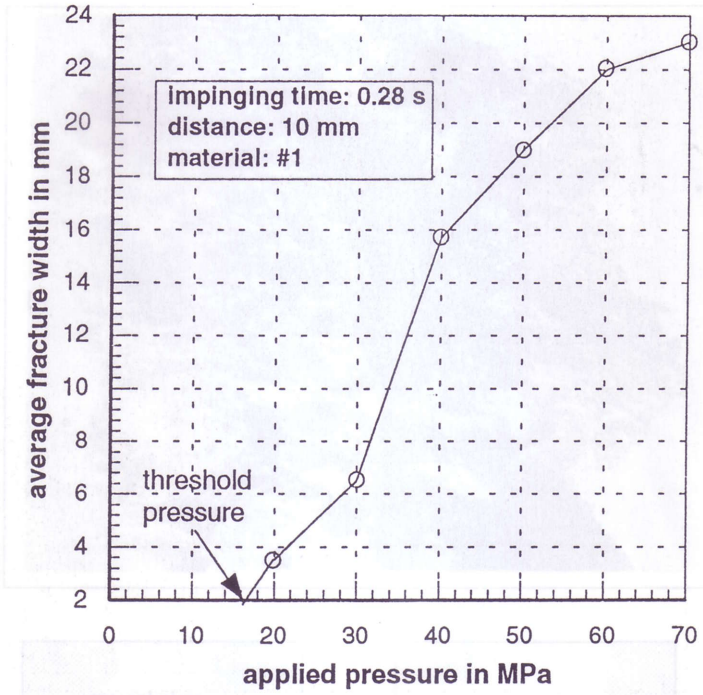

Fig. 5. Relation between applied pump pressure and average fracture width.

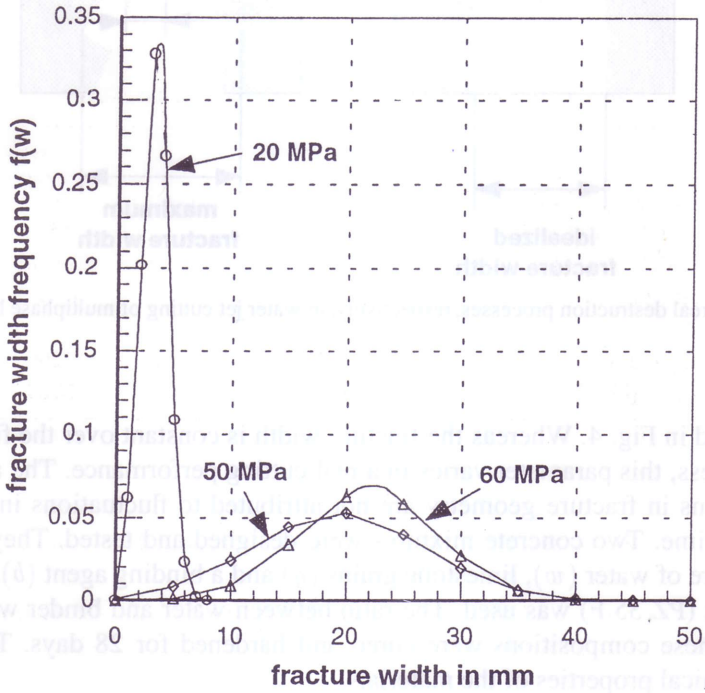

Fig. 6. Examples of fracture width distributions.

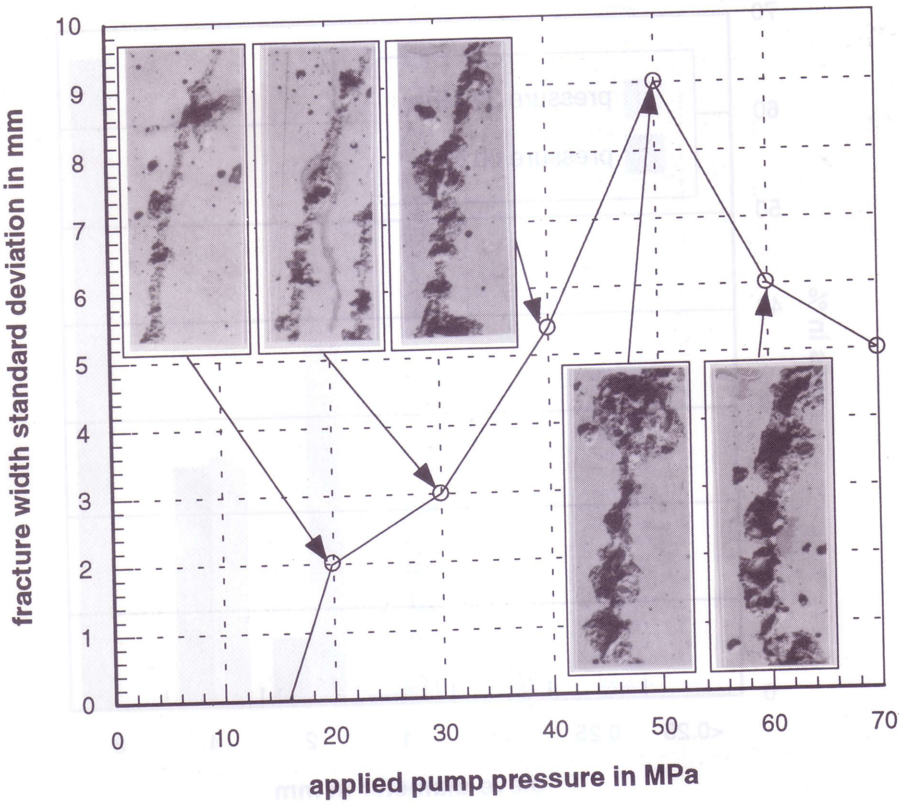

Fig. 7. Relation between applied pump pressure and fracture width deviation.

Table 1. Mechanical properties of the investigated materials

Parameter	Material # 1	Material # 2
Compressive strength [MPa]	21	39
Tensile strength [MPa]	2.1	4.5
Young's modulus [MPa]	19930	25463
Absorbed fracture energy [MJ/m^3]	14.5	65.1
Bulk density [kg/m^3]	2070	2290
Shear modulus [MPa]	8370	10690

and analyze it. Measurements of fracture width and fracture depth were carried out using conventional instruments.

Figure 7 shows examples of measured fracture width profiles. The standard deviation d_w was estimated using the equation

$$d_w = \sqrt{\frac{1}{n-1} \cdot \sum_{i=1}^{n} (w_i - w_M)^2}, \tag{4}$$

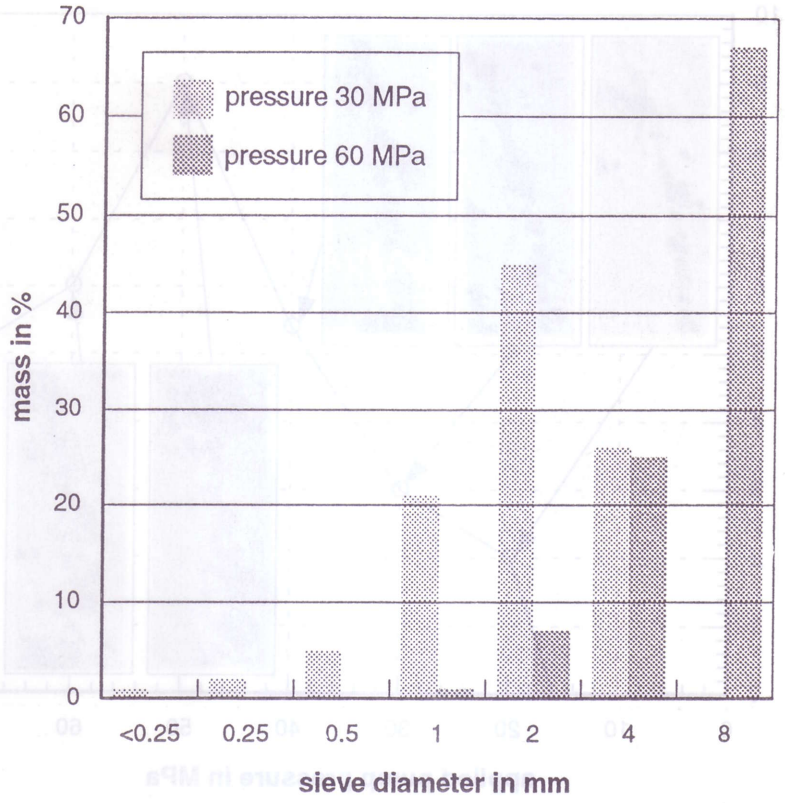

Fig. 8. Typical grain distributions of removed material samples.

where d_w is the standard deviation of the fracture width, w_M is the average value of the fracture width, and n is the number of measurements. Additionally, the removed particles were collected and their size distributions were estimated by sieve analysis. Typical samples of removed material particles are given in Fig. 8.

3. Experimental results

In Fig. 5 the relation between the applied pressure and the average fracture width is shown. The width increases linearly with rising pressure in the lower pressure range but it seems that a 'saturation' fracture width w_{MAX} exists, which may be identical with the maximum possible fracture width for the given material under the given conditions. The function asymptotically approaches this maximum value. Figure 6 shows typical fracture width distribution diagrams. It can be seen that the distribution can be described by a Gaussian Normal Distribution function as given by the equation

$$f(w) = \frac{1}{\sqrt{2 \cdot \pi} \cdot d_w} \cdot \mathrm{e}^{\frac{-(w-w_M)^2}{2 \cdot d_W^2}} . \tag{5}$$

In Fig. 7 the standard deviations of the fracture width distribution functions are plotted against the pump pressure, which can be understood as loading intensity. The function starts to increase at a pressure of about 20 MPa and is developed with a steady progress. The standard deviation rises with the intensity of loading. The specimen surface shows an adequate

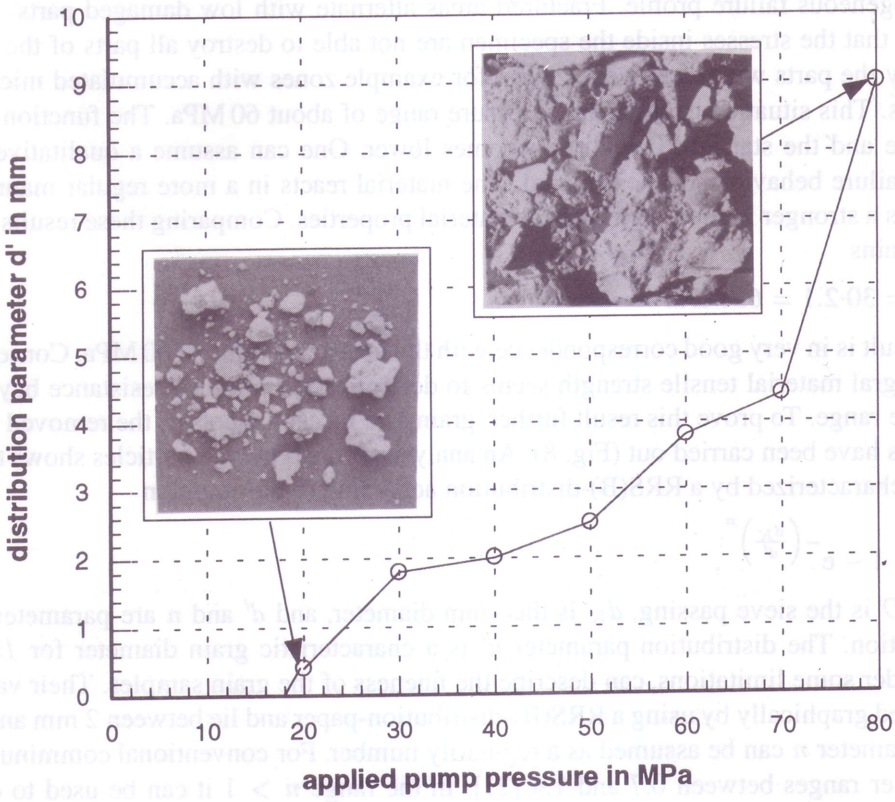

Fig. 9. Relation between applied pump pressure and the fineness parameter d'.

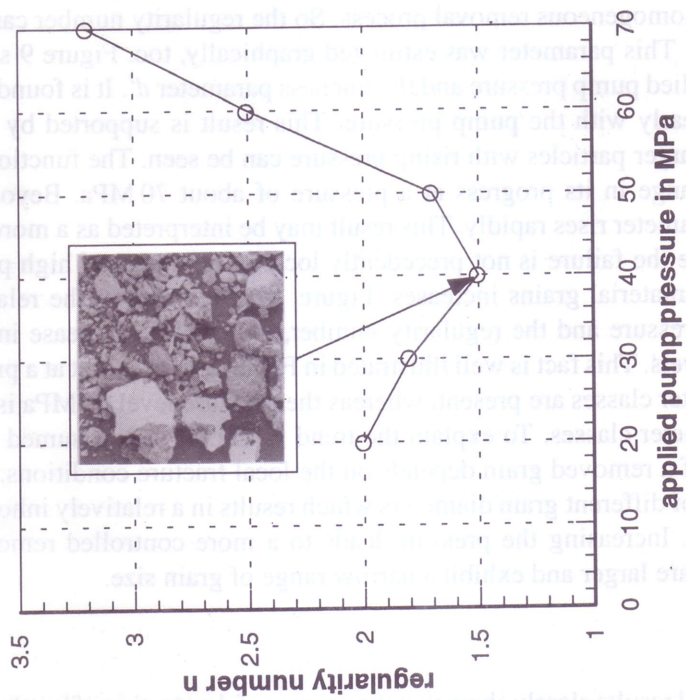

Fig. 10. Relation between applied pump pressure and the regularity parameter n.

inhomogeneous failure profile. Fractured areas alternate with low damaged parts. One can assume that the stresses inside the specimen are not able to destroy all parts of the material but only the parts with local weak zones, for example zones with accumulated microcracks or pores. This situation changes in a pressure range of about 60 MPa. The function starts to decrease and the standard deviation becomes lower. One can assume a qualitative change in the failure behaviour of the material. The material reacts in a more regular manner. This suggests a stronger influence of integral material properties. Comparing these results with (3) one obtains

$$p_{cr} = 30 \cdot 2.1 = 63\,\text{MPa}.$$

This result is in very good correspondence with the measured value of 60 MPa. Consequently, the integral material tensile strength seems to determine the material resistance beyond this pressure range. To prove this result further, grain size measurements of the removed material particles have been carried out (Fig. 8). An analysis of the removed particles shows that they can be characterized by a RRS(B)-distribution according to the equation

$$D = 1 - \mathrm{e}^{-\left(\frac{d_K}{d'}\right)^n}, \tag{6}$$

where D is the sieve passing, d_K is the grain diameter, and d' and n are parameters of the distribution. The distribution parameter d' is a characteristic grain diameter for $D = 0.63$ and, under some limitations, can describe the fineness of the grain samples. Their values are estimated graphically by using a RRS(B)-distribution-paper and lie between 2 mm and 9 mm. The parameter n can be assumed as a regularity number. For conventional comminution this parameter ranges between 0.7 and 1.4 [21]. In the range $n > 1$ it can be used to describe the homogeneity of the grain size distribution. The value for n is infinite if the grain sample consists of grains with identical diameters. Related to the present problem this would be valid in an idealized homogeneous removal process. So the regularity number can characterize the removal regime. This parameter was estimated graphically, too. Figure 9 shows the relation between the applied pump pressure and the fineness parameter d'. It is found that the diameter d' increases linearly with the pump pressure. This result is supported by Fig. 8 where the increase in the larger particles with rising pressure can be seen. The function in Fig. 9 shows a significant change in its progress at a pressure of about 70 MPa. Beyond this value the characteristic diameter rises rapidly. This result may be interpreted as a more integral fracture process. Because the failure is not precedently local in the range of high pressures, the size of the removed material grains increases. Figure 10 which shows the relation between the applied pump pressure and the regularity number, indicates an increase in the regularity at high pressure levels. This fact is well illustrated in Fig. 8. It is seen that at a pressure of 30 MPa five grain diameter classes are present, whereas the pressure level 60 MPa is characterized by three grain diameter classes. To explain the trend in Fig. 10 it is assumed that at low stress levels the size of a removed grain depends on the local fracture conditions. This should lead to a large range of different grain diameters which results in a relatively inhomogeneous grain size distribution. Increasing the pressure leads to a more controlled removal process. The removed grains are larger and exhibit a narrow range of grain size.

4. Discussion

The experimental results clearly show that the process of destruction of brittle multiphase materials by high energy water jets is characterized by effects of randomness and non-regularity.

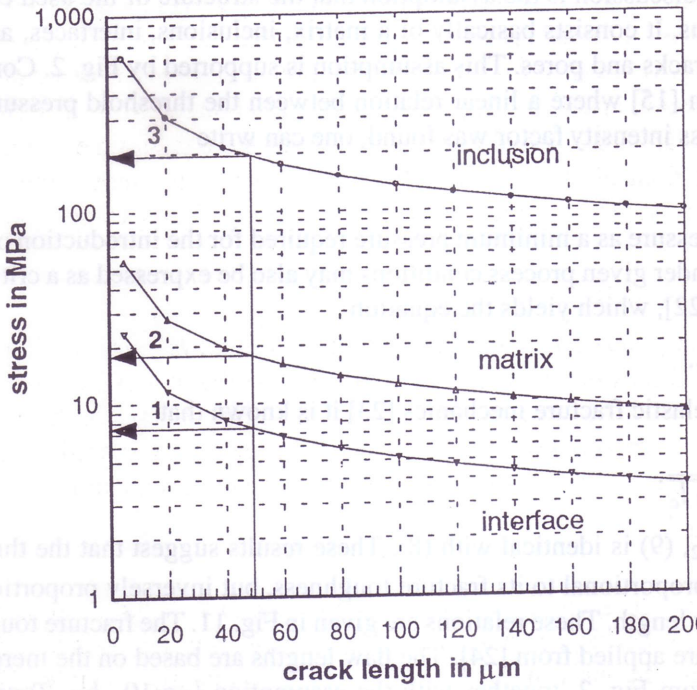

Fig. 11. Relation between fracture stress, crack length and local critical stress intensity factor.

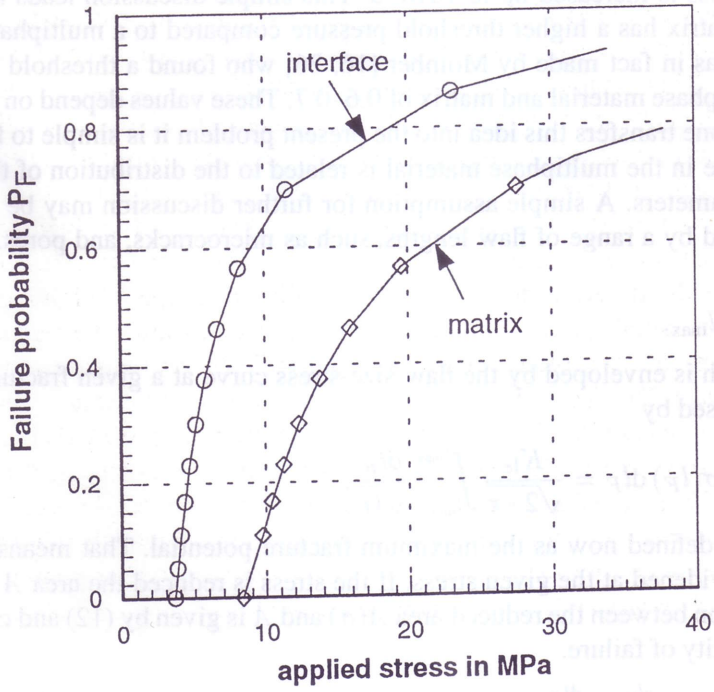

Fig. 12. Relation between fracture probability, applied stress and loading localization.

The basis of the discussion is the assumption that the structure of the used concrete samples is inhomogeneous. It consists basically of a matrix, inclusions, interfaces, and a network of flaws, as microcracks and pores. This assumption is supported by Fig. 2. Considering experimental results in [15] where a linear relation between the threshold pressures of rocks and their critical stress intensity factor was found, one can write

$$p_c = c_1 \cdot K_{\mathrm{Ic}}. \tag{7}$$

The threshold pressure as a minimum pressure required for the introduction of the failure in a given material under given process conditions may also be expressed as a critical stress inside a material flaw [22], which yields the equation

$$\sigma_c = C_2 \cdot K_{\mathrm{Ic}}. \tag{8}$$

From the linear elastic fracture mechanics [23] it is known that

$$\sigma_c = \frac{K_{\mathrm{Ic}}}{\sqrt{2 \cdot \pi \cdot l_c}}. \tag{9}$$

For $\frac{1}{\sqrt{2\pi \cdot l_C}} = C_2$, (9) is identical with (8). These results suggest that the threshold pressure of a material is proportional to its fracture toughness, but inversely proportional to the 0.5th power of the flaw length. These relations are given in Fig. 11. The fracture toughness values in this calculation are applied from [24]. The flaw lengths are based on the mercury penetration measurements from Fig. 2, together with the assumption $l_F \approx 10 \cdot b_F$. Typical critical flaw lengths for concretes are between 20 μm and 200 μm [25]. Figure 11 shows that the critical fracture stress depends on the local situation in the loaded area. For a given stress of 7.5 MPa, fracture occurs only in the interface between matrix and inclusion. A matrix failure can happen only if the stress is increased up to 18 MPa. This simple discussion leads to the conclusion that a plain matrix has a higher threshold pressure compared to a multiphase material. This observation was in fact made by Momber [16, 26] who found a threshold pressure relation between multiphase material and matrix of 0.6–0.7. These values depend on the sort of added inclusions. If one transfers this idea into the present problem it is simple to find that the non-regular fracture in the multiphase material is related to the distribution of the local material resistance parameters. A simple assumption for further discussion may be that the material is characterized by a range of flaw lengths, such as microcracks, and pores. This range may be

$$l_{\min} \leqslant l_F \leqslant l_{\max}. \tag{10}$$

The area which is enveloped by the flaw size-stress curve at a given fracture toughness can then be expressed by

$$A = \int_{l_{\min}}^{l_{\max}} \sigma(l_F)\, \mathrm{d}l_F = \frac{K_{\mathrm{Ic}}}{\sqrt{2 \cdot \pi}} \int_{l_{\min}}^{l_{\max}} \frac{\mathrm{d}l_F}{\sqrt{l_F}}. \tag{11}$$

The area A is defined now as the maximum fracture potential. That means that for (11) all flaws can be widened at the given stress. If the stress is reduced the area A will be reduced, too. The relation between the reduced area $A(\sigma)$ and A is given by (12) and can be interpreted as the probability of failure.

$$P_F = \frac{A(\sigma)}{A} = \frac{\int_{l_F(\sigma)}^{l_{\max}} \frac{\mathrm{d}l_F}{\sqrt{l_F}}}{\int_{l_{\min}}^{l_{\max}} \frac{\mathrm{d}l_F}{\sqrt{l_F}}}. \tag{12}$$

For $A(\sigma) = A$, one obtains $p_F = 1$. Equation (12) is graphically solved in Fig. 12. This figure shows two important relations. First, the probability of failure increases with the applied stress, and, second, the failure probability depends on the fracture toughness of the material phases. To obtain an average failure probability of $p_F = 0.5$ a stress of 7 MPa is necessary for the interface, whereas a stress of 18 MPa is necessary for the plain matrix. Also, two different 'threshold stresses' can be found. As estimated experimentally in [27], the water pressure on the bottom of a crack is about 20 percent of the applied stagnation pressure. Comparing the critical fracture stresses ($p_F = 0$) in Fig. 12 with the measured threshold pressures of the used materials (18 MPa for the multiphase concrete material, 40 MPa for a plain reference matrix) one obtains relations between 0.19 and 0.21 which are in excellent agreement with the values estimated in [27]. A regression of the functions in Fig. 12 leads to

$$p_F = a + b \cdot \ln \sigma. \tag{13}$$

It can be assumed now that the fracture width is related to the failure probability by

$$w = K \cdot p_F, \quad 0 \leqslant p_F \leqslant 1, \tag{14}$$

with $w = w_{\mathrm{MAX}}$ at $p_F = 1$. Combining (13) and (14), and assuming $p = k \cdot \sigma$ yields

$$w = K \cdot \left[a + b \cdot \ln \left(\frac{p}{k} \right) \right]. \tag{15}$$

This equation is able to describe the experimental estimated relation between the pump pressure and the average fracture width in Fig. 5. This equation may also be used to describe the fracture width standard deviation by plotting a group of lines for different local fracture parameters in the diagram. Probably, at a certain stress level, the space between these particular lines will be reduced. This stress level may be identical with the pump pressure in Fig. 7, where the standard deviation of the fracture width starts to drop. Here, further research is planned.

5. Conclusions

The conclusions from this investigation can be summarized as follows:

1. Cutting of multiphase materials with high pressure water jets is a highly localized process.
2. For the evaluation of the resistance of the materials in this kind of loading, the distribution of local material properties is of decisive significance in a pressure range up to 30-times the material tensile strength.
3. Beyond this pressure level the integral material properties characterize the failure behaviour of the material.
4. The width of the generated fracture is distributed over the loaded area as a Gaussian Normal Distribution.
5. The width of the generated fracture in the processed specimens is proportional to the local fracture probability which depends on the applied stress (pump pressure), the local fracture toughness, and the local microcrack distribution.
6. A semi-empirical model is developed to describe the relation between the pump pressure and the width of the generated kerf.

Acknowledgements

The authors are thankful to the Alexander-von-Humboldt Foundation, Bonn, and to the Center for Robotics and Manufacturing Systems, University of Kentucky, KY, for financial support. Also, they wish to thank the Institute of Material Sciences, University of Hanover, for supporting the experimental part.

References

1. R.J. Fowell and J. Martin, in *Jet Cutting Technology*, Kluwer Academic Publishers, Dordrecht (1992) 149–166.
2. M.M. Vijay, *International Journal of Surface Mining* 6 (1992) 1–9.
3. D.A. Summers, *Mining Engineer* 152 (1992) 45–51.
4. A. Momber, *Handbuch Druckwasserstrahl-Technik*, Beton Verlag, Düsseldorf (1993).
5. D.S. Shavlovsky, in *Proceedings 1st International Symposium on Jet Cutting Technology*, BHRA Fluid Engineering, Bedford (1972) 81–92.
6. K. Yanaida, in *Proceedings 2nd International Symposium on Jet Cutting Technology*, BHRA Fluid Engineering, Bedford (1974) 19–32.
7. C.E. Whiting, E.E. Graham and B. Ghorashi, *ASME Journal of Engineering for Industry* 112 (1990) 240–244.
8. G. Rehbinder, in *Proceedings 4th International Symposium Jet Cutting Technology*, BHRA Fluid Engineering, Bedford (1978) E1–E11.
9. H.J. Powell and S.P. Simpson, *International Journal of Rock Mechanics and Mining Science* 6 (1969) 353–364.
10. S.E. Forman and G.A. Secor, in *Proceedings 6th Conference on Drilling and Rock Mechanics*, Austin (1973) 163–174.
11. G. Rehbinder, *International Journal of Rock Mechanics and Mining Science* 14 (1977) 229–234.
12. J.L. Evers, D.L. Eddingfield and W.S. Man, in *Proceedings 7th International Symposium Jet Cutting Technology*, BHRA Fluid Engineering and National Research Council of Canada, Bedford (1984) 199–216.
13. J.L. Evers and D.L. Eddingfield, in *Proceedings 8th International Symposium Jet Cutting Technology*, BHRA Fluid Engineering, Bedford (1986) 237–248.
14. X. Yong, in *Proceedings 9th International Symposium Jet Cutting Technology*, BHRA Fluid Engineering and Water Jet Technology Society of Japan, Bedford (1988) 659–666.
15. J. Wiedemeier, *Flüssigkeitsfreistrahlen hoher Relativgeschwindigkeit und Bruchkinetik spröder Werkstoffe*, PhD dissertation, University of Hannover, Germany (1981).
16. A. Momber, *Untersuchungen zum Verhalten von Beton unter der Belastung durch Druckwasserstrahlen*, VDI-Verlag, Düsseldorf (1992).
17. A. Momber, *Materialwissenschaft und Werkstofftechnik* 13 (1992) 283–286.
18. A. Momber and H. Louis, *Materials and Structures* 27 (1994) 153–156.
19. A. Momber and R. Kovacevic, *Wear* 117 (1994) 55–62.
20. A. Momber, R. Kovacevic and J. Ye, *Tribological Transactions* (1994) to be printed.
21. H. Schubert, *Aufbereitung fester mineralischer Rohstoffe Bd. 1*, Deutscher Verlag für Grundstoffindustrie, Leipzig (1988).
22. P.P. Scott, W.G. Bearden and G.C. Howard, *Transactions of the AIME* 198 (1954) 111–114.
23. H. Blumenauer and G. Pusch, *Technische Bruchmechanik*, Deutscher Verlag für Grundstoffindustrie, Leipzig (1982).
24. B. Hillemeier, Bruchmechanische Untersuchungen zum Rißfortschritt in zementgebundenen Werkstoffen, PhD dissertation, University Karlsruhe (1976).
25. S. Mindess, in *Fracture Mechanics of Concrete*, Elsevier, Amsterdam (1983) 1–20.
26. A. Momber, in *Werkstoffwissenschaften und Bausanierung*, Expert Verlag, Böblingen (1992) 554–571.
27. M. Mazurkiewicz, J. White and G. Galecki, in *Proceedings 8th International Symposium Jet Cutting Technology*, BHRA Fluid Engineering, Bedford (1986) 189–193.